Available online at www.sciencedirect.com

ScienceDirect

journal homepage: www.intl.elsevierhealth.com/journals/dema

Properties of axially loaded implant–abutment assemblies using digital holographic interferometry analysis

Juraj Brozović[a,*], *Nazif Demoli*[b], *Nina Farkaš*[c], *Mato Sušić*[d], *Željko Alar*[e], *Dragana Gabrić Pandurić*[d]

[a] *Private dental office, Split, Croatia*
[b] *Institute of Physics, Zagreb, Croatia*
[c] *Private dental office, Zagreb, Croatia*
[d] *Department of Oral Surgery, School of Dental Medicine, Zagreb, Croatia*
[e] *Faculty of Mechanical Engineering and Naval Architecture, Zagreb, Croatia*

ARTICLE INFO

Article history:
Received 2 September 2013
Received in revised form
9 December 2013
Accepted 13 December 2013

Keywords:
Interferometry
Dental material
Materials testing
Loading
Biomechanics
Dental stress analysis
Dental implants
Dental implant–abutment design

ABSTRACT

Objective. The aim of this study was to (i) obtain the force-related interferometric patterns of loaded dental implant–abutment assemblies differing in diameter and brand using digital holographic interferometry (DHI) and (ii) determine the influence of implant diameter on the extent of load-induced implant deformation by quantifying and comparing the obtained interferometric data.

Methods. Experiments included five implant brands (Ankylos, Astra Tech, blueSKY, MIS and Straumann), each represented by a narrow and a wide diameter implant connected to a corresponding abutment. A quasi-Fourier setup with a 25 mW helium–neon laser was used for interferometric measurements in the cervical 5 mm of the implants. Holograms were recorded in two conditions per measurement: a 10 N preloaded and a measuring-force loaded assembly, resulting with an interferogram. This procedure was repeated throughout the whole process of incremental axial loading, from 20 N to 120 N. Each measurement series was repeated three times for each assembly, with complete dismantling of the implant-loading device in between. Additional software analyses calculated deformation data. Deformations were presented as mean values ± standard deviations. Statistical analysis was performed using linear mixed effects modeling in R's lme4 package.

Results. Implants exhibited linear deformation patterns. The wide diameter group had lower mean deformation values than the narrow diameter group. The diameter significantly affected the deformation throughout loading sessions.

Significance. This study gained *in vitro* implant performance data, compared the deformations in implant bodies and numerically stated the biomechanical benefits of wider diameter implants.

* *Corresponding author at*: Private dental office Selina Brozović, DMD, Getaldićeva 33, 21000 Split, Croatia. Tel.: +385 21 461090.
E-mail address: juraj.brozovic.dmd@gmail.com (J. Brozović).

0109-5641/$ – see front matter © 2013 Academy of Dental Materials. Published by Elsevier Ltd. All rights reserved.
http://dx.doi.org/10.1016/j.dental.2013.12.005

1. Introduction

The surgical placement of dental implants is the most predictable phase in implant dentistry resulting with successful integration in more than 98% of the cases [1,2]. The long term success of an integrated implant can be assessed by evaluating the surrounding bone level, peri-implant soft tissue, prosthetic superstructure and patient's overall satisfaction [3]. The objective clinical parameters mentioned are interdependent: a standard two-piece implant has an inevitable microgap at the prosthetic interface, thus facilitating bacterial colonization that may result in soft tissue inflammation and crestal remodeling [4,5]. Furthermore, functional loading propagates microgap enlargement [6] and can additionally influence the peri-implant tissue physiology.

Research on implant biomechanics associated load distribution with implant size and shape [7,8]. In finite element analysis (FEA) studies, an increase in implant diameter was demonstrated to cause an exponential decrease of peri-implant bone stress upon loading. In one study [8], the highest stress reduction exhibited (31.5%) was between the 3.6 mm and 4.2 mm diameter implants. Further enlargement of implant diameter resulted in a continuous drop in stress reduction. The same study, however, reported that increasing the implant length did not influence bone stress in the same order of magnitude; the reduction effect was significantly lower. Another observation pertaining to this issue noted that 80–100% of load induced stress was exhibited in the crestal 40% of the fixture, regardless of the implant length [7]. Collectively, these findings emphasize the importance of analysing the loading properties of the cervical part of an implant in the field of implant biomechanics.

A substantial number of studies have analysed the peri-implant bone stress; however, they seldom investigated the changes in the implant–abutment assembly itself [6,9–15]. Most of the analyses were based upon virtually simulated experiments, thus lacking empirical data pertinent for actual performance. In spite of many advantages, FEA can describe the behavior of real 3D structures only to an accuracy depending on the appropriate complexity of the virtual model, size of the mesh, displacement gradient variations and errors in input data. Digital holographic interferometry (DHI) enables a direct insight in rough surface deformation upon loading *in vitro* with submicron accuracy [16]. The method overcomes the mentioned problems by providing continuous, non-destructive and whole-field deformation measurements of actual specimens. Term 'digital' means the employment of a CCD sensor for recording holograms [17] which can then be stored in computer memory and reconstructed either numerically or optically [18,19].

To our knowledge, only a small number of studies used an interferometric approach for evaluating implant biomechanics [6,20,21]. Wahl et al. [6] studied the influence of load application on titanium implant–superstructure interface dislocation using electronic speckle pattern interferometry (ESPI). Three 4.1 mm diameter implants were connected to three different prosthetic superstructures and loaded with a 41.6 N force applied to the palatal cusps of the crowns at a 45° angle using a piezoelectric device. The screw retained superstructure dislocations at the implant–superstructure interfaces were analysed and quantified, resulting with a mean value of 0.27 μm gap formations. Chorres et al. [20] used holographic interferometry (HI) to compare the load distributions between fully-implant and tooth-implant supported fixed pontics. The authors used three 4.0 mm diameter titanium implants previously placed in the dog mandibles and compared the two types of fixed prostheses loaded with a 10 N force at anterior, midpoint and posterior positions. The qualitative analysis of the holograms obtained showed uniform deflection fringes in fully-implant supported pontics, whereas in case of tooth-implant pontics fringes were not present in dental abutments due to the higher displacement of the teeth than the capacity of the holography set up. Matsumoto et al. [21] investigated implant-induced stress concentration in monkey mandibles using HI. The authors placed a ceramic implant in the second molar position, supporting a fixed partial denture between the fixture and the first and second premolars. The double exposure technique was used to obtain holographic interferograms for various force applications to the superstructure. When vertically loaded at the second premolar point, the bone exhibited the highest stress concentration on the mesial aspect of the pontic, causing a detrimental effect on the bone.

To this date, there has not been an interferometric study that thoroughly analysed loading properties of different implant-abument assemblies. The purpose of this study was to obtain the interferometric patterns and analyse the deformations in the cervical portions of several implant–abutment assemblies under incremental axial loading by means of digital holographic interferometry. Additionally, our objective was to compare the loading properties of different implant–abutment assemblies based on their diameters.

2. Materials and methods

Experiments included 5 different titanium dental implant brands: Ankylos (Friadent, GmbH, Mannheim, Germany), Astra Tech (Astra Tech AB, Mölndal, Sweden), blueSKY (Bredent GmbH & Co. KG, Senden, Germany), MIS (MIS Implants Technologies Ltd., Bar Lev Industrial Park, Israel) and Straumann (Institut Straumann AG, Basel, Switzerland). Each brand was represented by a narrow and a wide diameter implant connected to a corresponding titanium abutment, as listed in Table 1.

2.1. *Loading device*

A special set of devices and accessories was designed, fabricated and tested at the Mechanical Properties Research Laboratory (Faculty of Mechanical Engineering and Naval Architecture, Zagreb, Croatia) throughout one year time period prior to this research (Fig. 1a). The basis for the implant loading assembly was a precision fabricated vertical vice with a heavy metal base that minimized undesired movements. First, a metal cylinder was mounted onto the vice bar. Secondly, a high precision digital dynamometer (HBM Kraftaufnehmer U1, Hottinger Baldwin Messtechnik GmbH, Darmstadt, Germany) was attached to the metal cylinder with a large diameter screw.

Table 1 – Implant–abutment assemblies used in the study.

Brand	Fixture	Abutment	Manufacturer
Ankylos	C/X A11 Ø 3.5 mm/L 11 mm C/X B11 Ø 4.5 mm/L 11 mm	Regular/X GH 3.0 mm/A0 Regular/X GH 3.0 mm/A0	Friadent GmbH, Mannheim, Germany
Astra Tech	Osseospeed TX S Ø 3.5 mm/L 11 mm Osseospeed TX S Ø 5.0 mm/L 11 mm	TiDesign 3.5/4.0 GH 3.0/4.5 mm TiDesign 4.5/5.0 GH 3.0/5.5 mm	Astra Tech AB, Mölndal, Sweden
blueSKY	Ø 3.5 mm/L 12 mm Ø 4.5 mm/L 12 mm	Esthetic L 0° GH 3.0 mm Esthetic L 0° GH 3.0 mm	Bredent GmbH & Co. KG, Senden, Germany
MIS	C1 Ø 3.75 mm/L 11.50 mm C1 Ø 5.0 mm/L 11.50 mm	Transgingival GH 3.0 mm Transgingival GH 3.0 mm	MIS Implants Technologies Ltd., Bar Lev Industrial Park, Israel
Straumann	Bone level RC Ø 3.3 mm/L 12 mm Bone level RC Ø 4.8 mm/L 12 mm	ST Anatomic GH 3.5 mm ST Anatomic GH 3.5 mm	Institut Straumann AG, Basel, Switzerland

The dynamometer was connected to a precision amplifier (GTM LT-Digitizer, Gassmann Testing and Metrology GmbH, Bickenbach, Germany) with an output to a personal computer. Furthermore, a custom made bearing table was screwed onto the dynamometer ensuring an even and straight platform for load bearing purposes. The clamping device, seated on the table, had a sliding metal plate which, when tightened, firmly secured an implant in its corresponding diameter

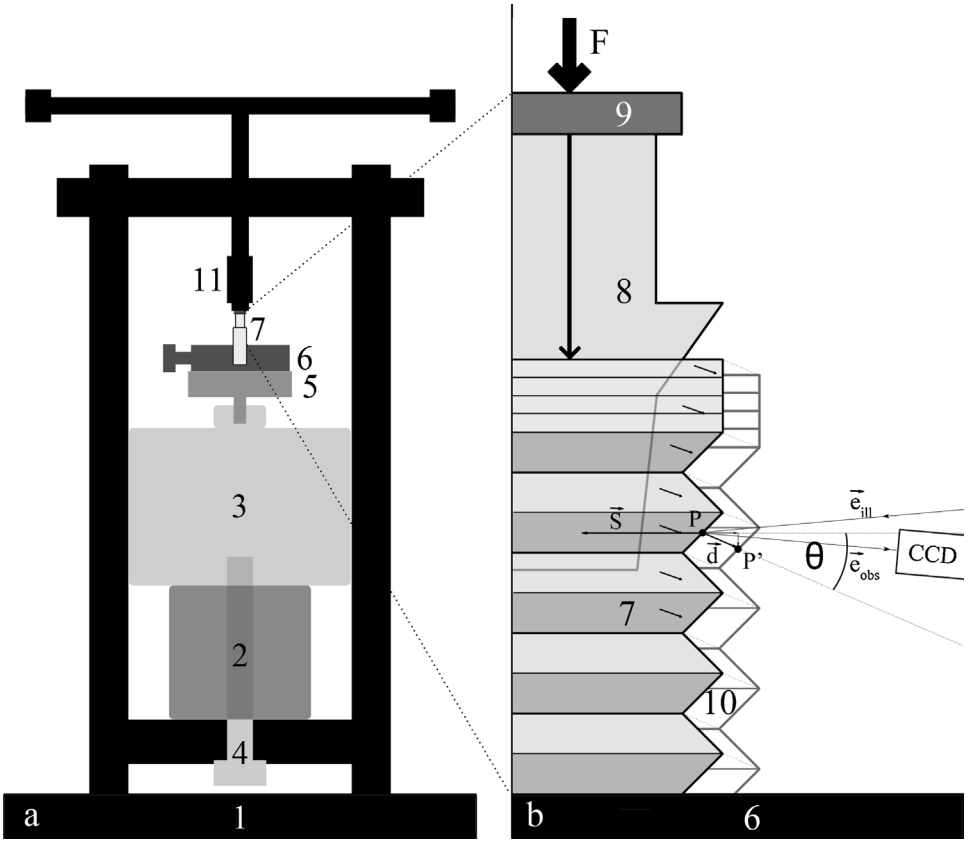

Fig. 1 – Implant loading device. (a) Device components. (b) Loaded implant components exposed to the laser beam (1 – vertical vice, 2 – metal cylinder, 3 – digital dynamometer, 4 – large diameter screw, 5 – bearing table, 6 – implant clamping device, 7 – dental implant, 8 – implant abutment, 9 – loading pin, 10 – deformed state implant, 11 – ram).

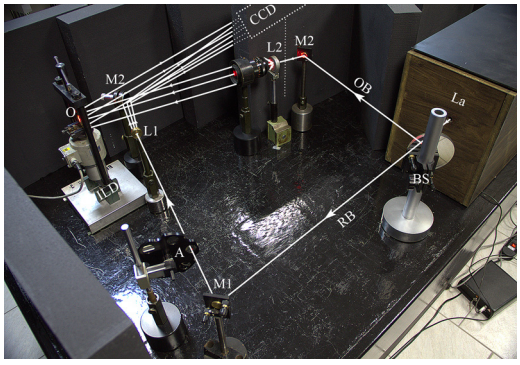

Fig. 2 – The interferometric setup (La – laser, BS – beam splitter, RB – reference beam, OB – object beam, M – mirror, L – lens, A – attenuator, ILD – implant loading device, O – object, CCD – charge-coupled device).

hole. This way, the implant position was always perpendicular to the surface of the clamping device. Every implant hole had an adjustable depth to ensure that all the implants protruded above the surface evenly, with 5 mm of their cervical portions exposed to the object beam (Fig. 1b). The abutments were tightened to their matching implants according to manufacturers' instructions using their corresponding torque wrenches. Individually crafted flat surface pins were seated into all the abutments studied in order to ensure an even pressure when loading implant–abutment assemblies. Gentle rotation of the screw press handle caused the ram to load an implant–abutment assembly with a force that was instantly recorded and visualized by the VN-Digitizer software (Gassmann Testing and Metrology GmbH, Bickenbach, Germany) on a personal computer.

2.2. *Experimental measurements*

All the experiments were performed at the Coherent Optics Laboratory (Institute of Physics, Zagreb, Croatia). A quasi-Fourier setup on a vibration-isolating table with a Spectra-Physics 25 mW helium–neon laser light source (wavelength: 632.8 nm) was used for digital holographic interferometry measurements (Fig. 2). The object beam was expanded and collimated to reflect from a part of the base (clamping device), the exposed cervical 5 mm of an implant and the abutment. A double recording technique was used for interferometric measurements. In the first recording, an implant–abutment assembly was always preloaded with a 10 N force in order to avoid unwanted movements upon ram seating on the abutment pin. After obtaining the first hologram, the implant–abutment assembly was loaded with a desired force and instantly recorded, resulting with the second hologram. Both holograms were superimposed and the obtained interferogram was reconstructed. This procedure was repeated throughout the whole process of incremental axial loading. Double exposure holograms of all implant–abutment assemblies were obtained for the following forces: 20 N, 30 N, 40 N, 50 N, 60 N, 70 N, 80 N, 90 N, 100 N, 110 N, and 120 N. Each series of measurements was repeated three times for each implant–abutment assembly, with complete dismantling of the implant-loading device in between series.

2.3. *Digital holographic interferometry*

Digital holographic interferometry (DHI) is a technique used for measuring displacement and/or deformation of a surface of investigated objects. Since the relative changes in the topology of the surface affect the phase of the incident coherent light, a series of holograms can be recorded to preserve different surface states. Then, two arbitrary holograms can be superposed and reconstructed. Their restored wave fronts interfere and form a fringe pattern that is modulating the reconstructed irradiance of the surface and also revealing the topology changes. By topology changes we refer to displacement vector, $\mathbf{d}(P)$, describing a change in location of a point P (new location is P') on the investigated surface. Generally, discrete-valued interferogram can be described by

$$I(m,n) = I_b(m,n) + V(m,n)\cdot\cos[\Delta\varphi(m,n)] + N(m,n) \quad (1)$$

where $I_b(m,n)$ is the background intensity, $V(m,n)$ is the fringe contrast (also, visibility of fringes), $\Delta\varphi(m,n)$ is the phase difference between two holograms, and $N(m,n)$ is an additive noise. Thus, the task is to find $\mathbf{d}(P)$ values for the entire surface from the $I(m,n)$ values. Two restrictions concerning the Eq. (1) are obvious: (i) the phase $\Delta\varphi(m,n)$ can only be evaluated up to 2π due to the periodicity of a cosine function and (ii) since the cosine function is even, the phase $\Delta\varphi(m,n)$ can be evaluated merely up to a sign. Less obvious but extremely important is influence of noise $N(m,n)$ on the $I(m,n)$ values. Many disturbances contribute to noise such as vibrations, thermal electronics noise, speckle noise, *etc.* Moreover, microscopic variations in the loading conditions affect the stress distribution within a sample and also variations in $\mathbf{d}(P)$ values. Finally, the insufficient sampling rate conditions (undersampling) lead to the loss of information due to the frequency folding or aliasing errors [22]. All these disturbances imply that more independent measurements for the same situation are needed to minimize the effect of noise.

For quantitative evaluation, the relation between the observed phase difference $\Delta\varphi(m,n)$ and the displacement vector $\mathbf{d}(P)$ is given by

$$\Delta\varphi(m,n) = \frac{2\pi}{\lambda}\mathbf{S}(P)\cdot\mathbf{d}(P) \quad (2)$$

where λ is the wavelength and $\mathbf{S}(P)$ is the sensitivity vector of a point P. The sensitivity vector is defined as $\mathbf{S}(P) = \mathbf{e}_{ill}(P) - \mathbf{e}_{obs}(P)$, *i.e.* as subtraction of two unit vectors indicating the illumination and observation directions (Fig. 1.b), where in general $\mathbf{S}(P)\cdot\mathbf{d}(P) = \left|\mathbf{e}_{ill}(P) - \mathbf{e}_{obs}(P)\right|\left|\mathbf{d}(P)\right|\cos\vartheta(P)$, and where the bracket $|\cdot|$ denotes the modulus operation. The angle $\vartheta(P)$ is determined by the displacement vector and the bisector of the illumination and viewing directions. The variations of the sensitivity vector across the investigated surface are possible due to the illumination conditions [23].

In general case, the phase difference depends on the component of the displacement vector projected to the sensitivity direction. In laboratory work it is convenient to start

interferometric measurements with a certain 'a priori' knowledge concerning the object under test and the loading conditions. Thus, if the displacement direction is known and the experimental arrangement allows the sensitivity direction to be aligned approximately collinear with the displacement direction, then $\left|\mathbf{e}_{ill}(P) - \mathbf{e}_{obs}(P)\right| = 2$ and the displacement value at the position (m,n) is

$$d(m,n) = \frac{\lambda}{4\pi}\Delta\varphi(m,n) \tag{3}$$

As discussed before, continuous phase information $\Delta\varphi(m,n)$ is sampled in a discrete wrapped data $\Delta\varphi_w(m,n)$ due of the periodic nature of the interfering waves. Therefore, if the true phase value is outside the basic interval $[-\pi,\pi)$, the observed (measured) value, $\Delta\varphi_w(m,n)$, is wrapped into this interval, or

$$\Delta\varphi(m,n) = \Delta\varphi_w(m,n) + 2\pi k(m,n) \tag{4}$$

where $k(m,n)$ is an integer. Taking into account the effects described by Eq. (4) as well as of various possible disturbances, the displacement value can be described as

$$d(m,n) = \frac{\lambda}{4\pi}[\Delta\varphi_w(m,n) + 2\pi k(m,n) + \delta\varphi(m,n)] \tag{5}$$

where $\delta\varphi(m,n)$ describes variation in detected phase. Relation (5) represents a basis for analyzing interferogram information.

2.4. *Interferogram analysis*

For the purpose of interferogram analyses, we have used the IDEA software (University of Technology, Graz, Austria). The holograms acquired at two different states of the implants, the preloaded and the deformed, were subtracted and Fast Fourier Transformed (FFT) to obtain the complex reconstruction of interferograms. The phase of the calculated modulo 2Π data from the cervical portion of dental implants was unwrapped using the discrete cosine transform (DCT) to recover the absolute phase. The calculation from phase data was exported in ASCII-format and transformed to exhibit the deformations at the micron scale (Fig. 3).

2.5. *Statistical analysis*

Deformations were presented as mean values ± standard deviations of the replicate experiments for each implant–abutment assembly for a corresponding force. Deformation values were box-plot transformed and demeaned. The assessment of the significance in deformation difference between the narrow and wide diameter assemblies was performed in R Statistical Software (R Core Team, Foundation for Statistical Computing, Vienna, Austria, 2012) using linear mixed effects modeling in R's lme4 package with implant brand considered as a random effect and deformation, load and diameter as fixed effects.

3. Results

The distinctive interferometric pattern of incremental out-of-plane deformation in the implant neck is presented in Fig. 4. Assemblies were divided into two groups: the narrow and the wide diameter group. Average deformation values of implant–abutment assemblies upon loading with respective forces are shown in Tables 2 and 3.

In the narrow diameter group, deformations ranged from 0.69 μm to 7.76 μm. Straumann implants exhibited the lowest starting deformation in the loading series (0.69 μm), at 20 N axial force. MIS implants, the largest in diameter among the narrow group, showed the lowest deformation throughout 30 N (0.89 μm) and 40 N (1.60 μm) forces, with a deformation value leap in between 40 N and 50 N (2.67 μm), where it exhibited the highest deformation. Ankylos implants showed the least deformation at 50 N (2.43 μm). Astra had the highest starting deformation in the series, however, it exhibited the lowest deformation streak from 60 N (2.69 μm) to 100 N (4.51 μm). Although smallest in diameter, at 110 N (5.19 μm) and 120 N (6 μm), Straumann showed the lowest deformation, while MIS (7.76 μm) and blueSKY (7.68 μm) implants exhibited the highest deformation values.

In the wide diameter group, deformations ranged from 0.47 μm to 5.20 μm. Astra showed the least starting deformation at 20 N (0.47 μm), followed by Straumann at 30 N (0.64 μm). Furthermore, Astra exhibited the lowest deformation streak from 40 N (1 μm) to 70 N (1.98 μm). Straumann had the lowest deformation value at 80 N (2.43 μm). Although smallest in diameter in the wide diameter group, blueSKY and Ankylos showed the least deformation at 90 N (3.09 μm and 3.10 μm, respectively), whereas Astra, MIS and Straumann performed nearly equally (3.28 μm, 3.28 μm and 3.30 μm, respectively), exhibiting higher deformation values. However, Astra showed the lowest deformation throughout 100 N and 110 N (3.14 μm) forces. At peak force, 120 N, MIS exhibited the least deformation (4.10 μm), while blueSKY showed the highest value (5.20 μm).

All of the assemblies included in the study exhibited linear deformation patterns throughout the implant body as well as throughout the incremental axial loading sessions. The linear regression lines for each assembly are shown in Fig. 5. Assemblies showed a tendency of grouping based on their diameters where the 3.3 mm, 3.5 mm and 3.75 mm diameters (narrow diameter group) had higher overall deformation values than the 4.5 mm, 4.8 mm and 5.0 mm diameters (wide diameter group). Group difference in deformation is shown in Fig. 6, where the wide diameter group had lower mean deformation values than the narrow diameter group. The more acute angle of the regression line in the wide diameter group showed that the wider implants were less influenced by the increase of loading force.

Linear mixed-effects modeling was performed using R's lme4 package. The inspection of residual plots did not show any obvious deviations from homoscedasticity and normality. The implant diameter in implant–abutment assemblies significantly affected the deformation values throughout the loading series (SE = 0.083; $t = -6.237$; $p < 0.001$).

4. Discussion

This study employed digital holographic interferometry in deformation analysis of different implant–abutment

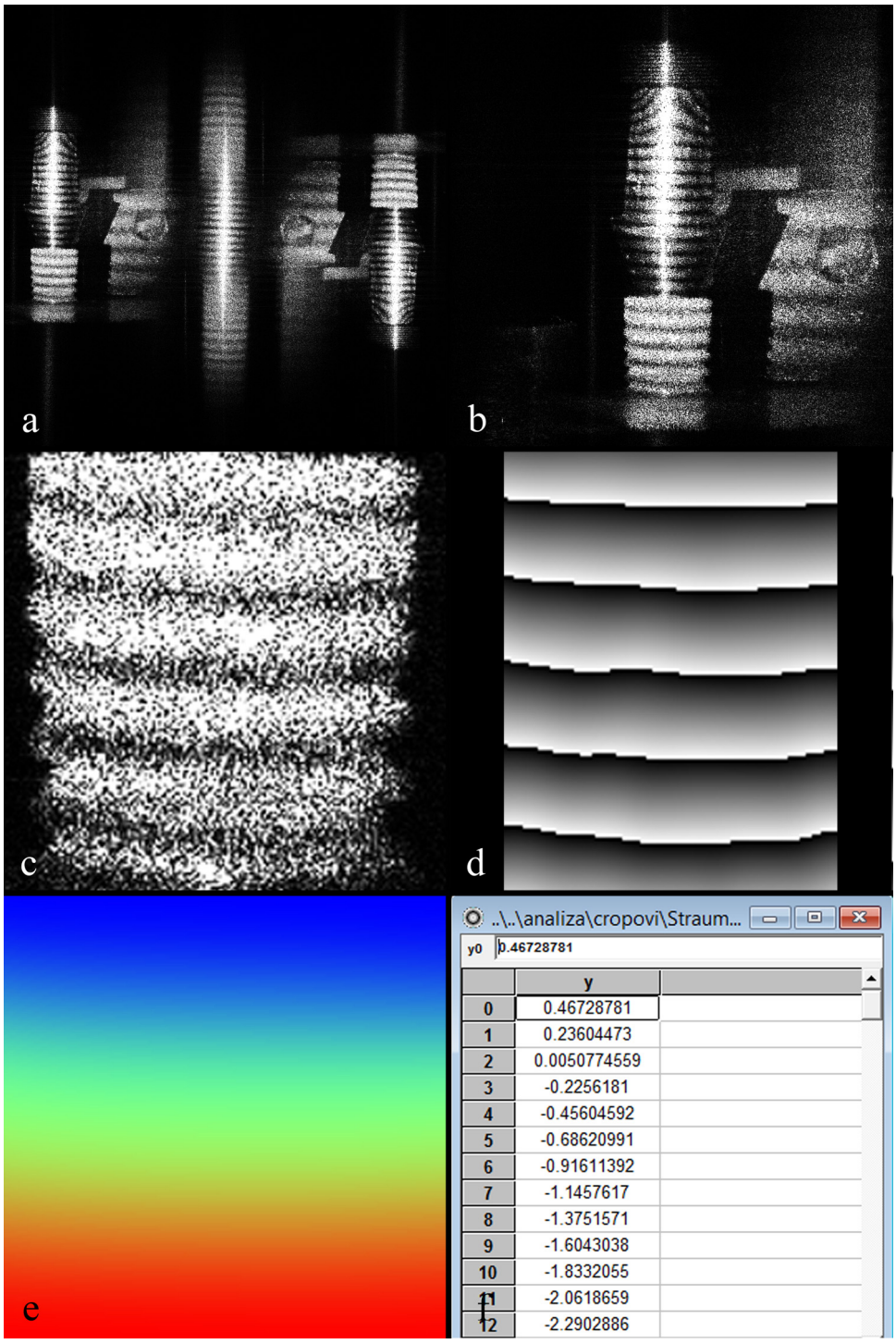

Fig. 3 – An example of deformation data extraction. (a) Reconstructed interferogram. (b) Interferometric appearance of implant–abutment assembly. (c) Cervical 5 mm of implant cropped. (d) Calculated modulo 2Π data from cervical portion. (e) Discrete cosine transform phase unwrapping. (f) Phase deformation throughout implant body.

assemblies. It challenged the effect of implant diameter on the extent of deformation throughout different loading conditions.

Preliminary measurements of repetitive loading in random specimens resulted with consistent results for the forces used in this research in terms of interferometric fringe counts. Relying on the findings of Wahl et al. [6], we have considered a 10 N preload suitable for the first hologram recording. At higher forces in the second hologram, fringes became denser and ultimately indistinguishable when exceeding forces greater than 120 N, the highest force used in the final loading series. A difference in interferometric pattern was noted when applying a 10 N higher force than a previous one, making it the incremental value between measurements. These

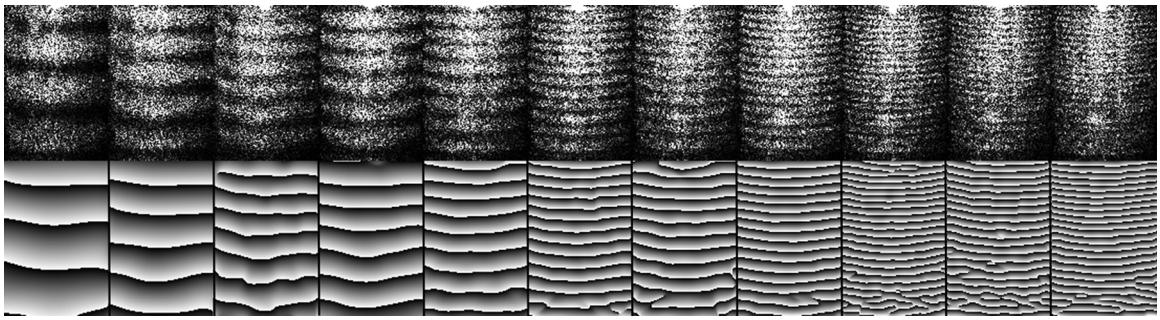

Fig. 4 – Interferometric appearance of incremental loading in the implant neck.

Table 2 – Load induced deformations of narrow diameter implant–abutment assemblies.

Force (N)	Ankylos 3.5 mm		Astra 3.5 mm		BlueSKY 3.5 mm		MIS 3.75 mm		Straumann 3.3 mm	
	Average (μm)	St. dev. (μm)	Average (μm)	St. dev. (μm)	Average (μm)	St. dev. (μm)	Average (μm)	St. dev. (μm)	Average (μm)	St. dev. (μm)
20	0.86	0.28	1.24	0.27	1.01	0.21	0.91	0.30	0.69	0.03
30	1.73	0.20	1.21	0.21	1.67	0.14	0.89	0.17	1.60	0.11
40	1.84	0.29	1.90	0.22	2.16	0.25	1.60	0.26	1.71	0.34
50	2.09	0.14	2.43	0.42	2.59	0.44	2.67	0.26	2.27	0.34
60	2.80	0.29	2.69	0.58	3.37	0.34	2.98	0.69	3.07	0.34
70	3.93	0.35	3.19	0.57	3.83	0.21	4.25	0.57	3.65	0.89
80	4.13	0.33	3.38	0.48	4.38	0.23	4.80	0.44	4.27	0.87
90	4.57	0.52	3.99	0.91	5.20	0.29	5.17	0.63	4.13	0.86
100	5.98	0.99	4.51	1.34	5.22	0.60	5.94	0.48	4.78	0.23
110	5.54	1.33	5.74	1.03	7.22	0.46	7.40	1.29	5.19	0.21
120	6.33	1.16	6.58	1.55	7.68	0.25	7.76	1.40	6.00	0.90

observations indicated that digital holographic interferometry was suitable for obtaining the specific force-related interferometric patterns for a whole series of loading from 20 N to 120 N, thus confirming effectivity of the method. Moreover, this force loading span was considered appropriate for studying implant biomechanics regarding the observations by Dittmer et al. [24] where average bite forces ranged from 20 N to 120 N. In the assessment of the implant diameter effect, linear mixed effects modeling analysed diameters as they were (*e.g.* 3.3 mm, 3.75 mm, *etc.*), rather than analysing them divided into narrow and wide diameter groups. This way, a more objective result was obtained. As expected, the findings of this study suggest that implant diameter considerably influences its susceptibility to deformations. When taking into consideration these results and the linear regression of assemblies divided into narrow and wide diameter groups, it appears reasonable that wide diameter implants exhibit significantly less deformation when incrementally loaded, and could sustain greater forces in the oral environment.

The rationale for studying the cervical 5 mm of a dental implant was due to the fact that most of the stresses occurred in that portion of the implant [7]. The interferograms in the preliminary measurements showed inconsistent and disparallel fringes upon direct loading of the implant abutments. The seating of individually crafted flat surface pins into the corresponding abutments was thus necessary to achieve balanced

Table 3 – Load induced deformations of wide diameter implant–abutment assemblies.

Force (N)	Ankylos 4.5 mm		Astra 5.0 mm		blueSKY 4.5 mm		MIS 5.0 mm		Straumann 4.8 mm	
	Average (μm)	St. dev. (μm)	Average (μm)	St. dev. (μm)	Average (μm)	St. dev. (μm)	Average (μm)	St. dev. (μm)	Average (μm)	St. dev. (μm)
20	0.51	0.11	0.47	0.09	0.52	0.06	0.60	0.12	0.49	0.11
30	0.81	0.23	0.73	0.27	0.89	0.14	0.82	0.06	0.64	0.07
40	1.43	0.07	1.00	0.27	1.11	0.03	1.27	0.09	1.27	0.35
50	1.70	0.13	1.29	0.36	1.48	0.07	1.66	0.06	1.74	0.23
60	2.02	0.32	1.34	0.20	1.89	0.13	2.09	0.20	1.90	0.21
70	2.44	0.32	1.98	0.31	2.19	0.27	2.07	0.08	2.15	0.22
80	2.80	0.61	2.64	0.18	2.69	0.34	2.66	0.27	2.43	0.21
90	3.10	0.32	3.28	0.34	3.09	0.21	3.28	0.21	3.30	0.33
100	4.16	1.04	3.59	1.05	4.24	0.70	3.88	0.16	3.92	0.48
110	4.73	1.17	3.14	0.40	4.78	0.34	4.41	0.13	4.74	0.53
120	5.03	1.27	4.32	0.86	5.20	0.19	4.10	0.08	5.04	0.06

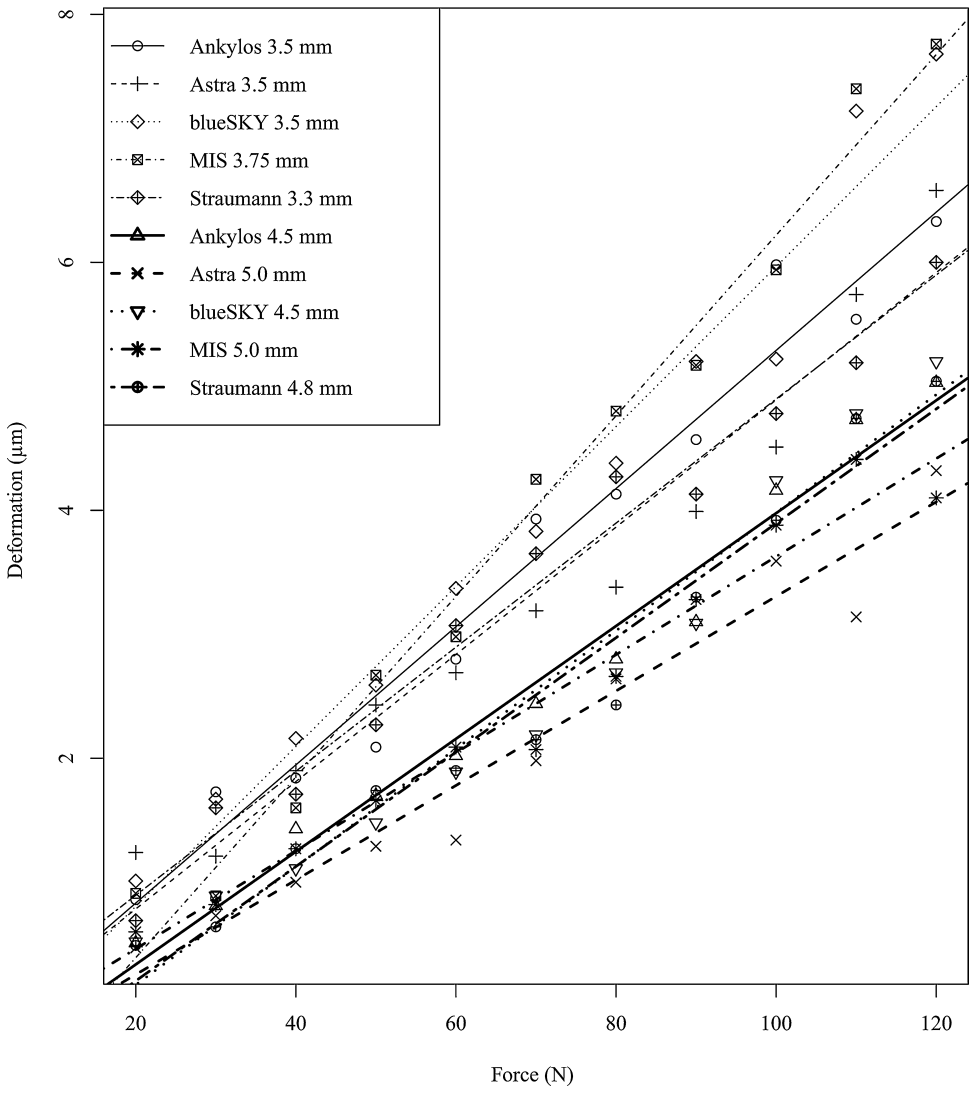

Fig. 5 – Linear regression lines for different implant–abutment assemblies under incremental loading.

loading conditions and consistent interferograms in repetitive measurements. Since the sensitivity vector of a point located at the implant surface was perpendicular to the force direction (Fig. 1b), the reconstruction ideally showed the widening of the implant neck. In a study by Semper et al. [25] authors have noted vertical alterations in implant–abutment complexes ranging from 1 to 83 μm when repeatedly disassembled and reassembled. In our study we have decided to disregard the mentioned alterations upon dismantling in between the loading sessions due to force direction being strictly axial. Therefore, the possible changes in height did not interfere with our measurements.

Deformation data gathered should not be considered as the actual deformation value upon loading with a specific force as in Tables 2 and 3, *e.g.* the 50 N loading force interferogram does not show the deformation of the implant for the specified force, it rather exhibits the difference in deformations between the preload force (10 N) and the force used in the recording of the second hologram (50 N). Deformation regression lines for all implants (Fig. 5) grouped based on their diameters. Thus an additional group regression was shown in Fig. 6, clearly justifying the assignments to each group. As the axial loading forces rose, the diameter group differences in implant deformations became more obvious.

The differences among implant brands were not assessed due to (i) low number of specimens investigated, and (ii) variability in obtained results (as seen in standard deviation values) depending on the previously mentioned variations of the sensitivity vector across the implant body. In order to compare different implant brands, a more extensive study should be carried out on a significantly higher number of specimens. Therefore, the implant brand was assigned to random effects in our analysis.

Wahl et al. [6] carried out series of one-dimensional interferometric measurements of implants subjected to linear increasing forces. The authors noted homogeneous deformations of implants. Our observations noted linear deformation patterns proportional to the application of incremental loads which concurs with this research. Another point at which our study shares the stance with the research mentioned is the

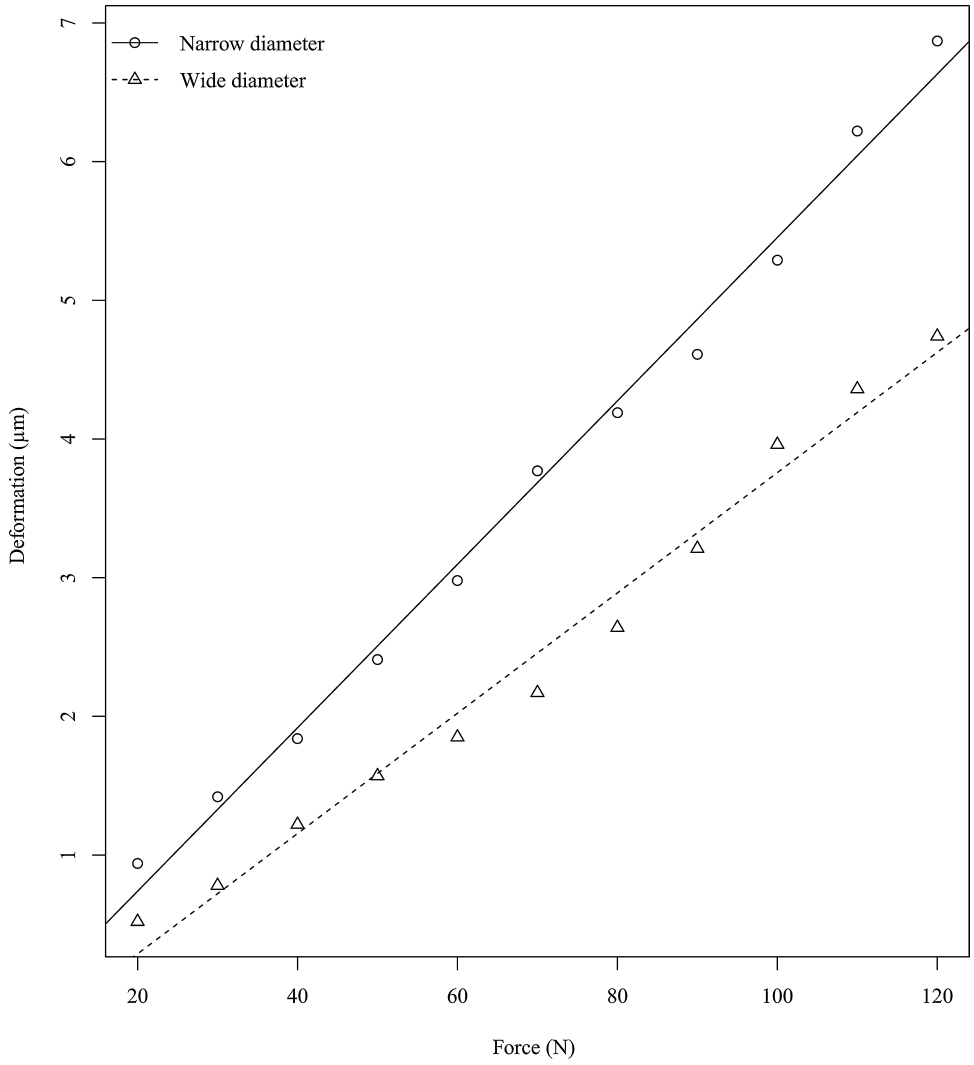

Fig. 6 – Linear regression lines for incremental loading of different diameter groups.

verdict that interferometric techniques can be effectively used in the field of implantology as direct *in vitro* testing modalities as opposed to indirect computer-supported finite element analyses. However, these more common analyses obtain less variable data in a more convenient way. Therefore, both methods present valuable sources of deformation data, and should be subjected to further comparison and evaluation in order to gain more objective results regarding true clinical performance.

Chorres et al. [20] observed *in vitro* static loading of tooth-implant and fully-implant supported fixed prostheses with interferometric method. A specific pattern in the implant body and dental prostheses was noted in case of fully-implant supported cases where horizontal fringes were present. The implant–abutment assemblies in our study showed the same horizontal fringe patterns when loaded with axially directed forces. The study mentioned was based solely on a qualitative comparison of holograms, whereas in the present study we have incorporated additional software analyses which enabled us to compare the data quantitatively as well. This was applicable due to the fact that we have used a digital holographic approach in interferometry with direct exporting of data to the analysis software. However, they have analysed implant-supported prosthetics, while our study dealt only with out-of-plane changes at the implant–abutment level.

Finite element analysis studies on implant biomechanics [8–15] focused on stresses in the peri-implant area. Al-Sukhun et al. [26–28] studied functional patterns of mandibular strain and deformation in implant treated patients *in vivo* and *in vitro*. The authors noted mandibular medial convergence values ranging from 11 μm to 109 μm during functional movements. Moreno et al. [29] employed an interferometric approach (ESPI) to visualize physiologically induced mechanical stress in the human mandible. It enabled a semi qualitative approach in gaining useful information despite of heterogeneity and anisotropy of the material studied, adding to the value of the method. The shortcoming of the present study may be that it focused on the stresses that occur in the implant–abutment assembly itself with a fully quantitative approach, not taking into consideration the surrounding tissue.

Baggi et al. [30] used FEA to assess the influence of implant dimensions on surrounding bone stress under static load

application. Their findings suggested that the selection of a wider implant diameter may contribute more to the bone overload risk control than implant length. Additionally, authors noted the worst load transmission to the bone in the maxillary molar region. Himmlova et al. [8] observed a significant decrease in peri-implant-neck bone stress when loading wider diameter implants, regardless of length. Despite the limited scope of the present study, our results may supplement these findings with similar observations at the implant level, where diameter increase led to a significant decrease in implant deformation. Similar results were obtained in a study by Qian et al. [31] where authors investigated stress and strain values in both bone and implants. Their comparison of 3.7 mm and 5.2 mm implants in various loading conditions can be directly related to our research, since the authors recorded the stresses occurring in the implant body that were diameter-dependant in a similar manner as the deformation in our study. Furthermore, a more beneficial performance of wider implants in stress and strain distribution in the surrounding bone was noted. Studies regarding bone remodeling have also engaged the implant diameter issue. Winter et al. [32] detected minor micromotion in the cervical part of a model of an osseointegrated implant in the range of 0.75 μm. Ojeda et al. [33] studied the microdamage in the surrounding bone caused by the same part of an implant, deeming the reduction in implant diameter "counterproductive to its stability". Our study may add to further elucidation of this issue by presenting the more pronounced cervical widening of narrow diameter implants. In a biomechanical response study, Chou et al. [34] have noted a more even and higher distribution of bone strain associated with wide diameter implants when compared to narrow diameter implants. Taking into consideration the aforementioned results, we can assume that wider implants both dissipate the masticatory force better and experience less deformations *in vitro*.

Our findings may aid the clinician in dealing with demanding cases involving high masticatory forces, where excessive deformation in implant body could lead to a mechanical failure. This study does not engage the peri-implant bone stress issue, it rather determines the beneficial mechanical properties of wider diameter implants *per se*.

Further limitations of this study are the variabilities between repeated recordings due to the deviations of the sensitivity vector across the implant surfaces and the material of the clamping device. The clamping device had a different elastic modulus than living bone, thus influencing the interferometric appearance of loaded implant–abutment assemblies. However, the material may not present an issue when comparing different multi-unit implant-borne prosthetics in the same clamping device, which can be analysed in future quantitative interferometric studies. Direct insight in multiple implant anchor and superstructure load distributions may present valuable data with direct clinical implications.

5. Conclusions

Based on 660 recorded holograms, resulting with 330 interferograms and further extensive software analyses, this interferometric study gained *in vitro* data denoting the extent of deformation for ten implant–abutment assemblies under incremental axial forces and numerically stated the biomechanical benefits of wider diameter implants. Statistical analysis showed the significant effect of implant diameters on deformation values. The applicability of the method in assemblies loaded with oblique forces is to be investigated as the next step in the interferometric analysis of dental implants.

Acknowledgements

This work was supported by the Croatian Ministry of Science, Education and Sports (project No. 035-0352851-2854). To Nenad Medić at Fitzwilliam College, Cambridge, for his kind assistance in statistical analysis. To Professor Jakob Woisetschläger at the Institute for Thermal Turbomachinery and Machine Dynamics, Graz, for his kind assistance in interferogram analysis. To Professor Vjekoslav Jerolimov on his kind assistance in technical preparations. To Pandent Ltd. (Ankylos), Novodent Ltd. (Astra Tech), Bredent Ltd. (blueSKY), S.D. Informatika Ltd. (MIS) and Sanitaria Ltd. (Straumann) for implant–abutment assemblies used in this research.

REFERENCES

[1] Misch CE, Misch-Dietsh F, Silc J, Barboza E, Cianciola LJ, Kazor C. Posterior implant single-tooth replacement and status of adjacent teeth during a 10-year period: a retrospective report. J Periodontol 2008;79:2378–82.
[2] Misch CE, Steignga J, Barboza E, Misch-Dietsh F, Cianciola LJ, Kazor C. Short dental implants in posterior partial edentulism: a multicenter retrospective 6-year case series study. J Periodontol 2006;77:1340–7.
[3] Papaspyridakos P, Chen CJ, Singh M, Weber HP, Gallucci GO. Success criteria in implant dentistry: a systematic review. J Dent Res 2012;91:242–8.
[4] Ujiie Y, Todescan R, Davies JE. Peri-implant crestal bone loss: a putative mechanism. Int J Dent 2012;2012:742439.
[5] Scarano A, Assenza B, Piattelli M, Iezzi G, Leghissa GC, Quaranta A, et al. A 16-year study of the microgap between 272 human titanium implants and their abutments. J Oral Implantol 2005;31:269–75.
[6] Wahl G, Lang H. Deformation at the implant interface to prosthetic superstructure: an interferometric approach. Clin Oral Implants Res 2004;15:233–8.
[7] Misch CE. Implant body size: a biomechanical and esthetic rationale. In: Misch CE, editor. Contemporary implant dentistry. St. Louis: Mosby; 2008. p. 164–5.
[8] Himmlova L, Dostalova T, Kacovsky A, Konvickova S. Influence of implant length and diameter on stress distribution: a finite element analysis. J Prosthet Dent 2004;91:20–5.
[9] Yamanishi Y, Yamaguchi S, Imazato S, Nakano T, Yatani H. Influences of implant neck design and implant–abutment joint type on peri-implant bone stress and abutment micromovement: three-dimensional finite element analysis. Dent Mater 2012;28:1126–33.
[10] Freitas-Junior AC, Rocha EP, Bonfante EA, Almeida EO, Anchieta RB, Martini AP, et al. Biomechanical evaluation of internal and external hexagon platform switched implant–abutment connections: an in vitro laboratory and three-dimensional finite element analysis. Dent Mater 2012;28:218–28.

[11] Li T, Yang X, Zhang D, Zhou H, Shao J, Ding Y, et al. Analysis of the biomechanical feasibility of a wide implant in moderately atrophic maxillary sinus region with finite element method. Oral Surg Oral Med Oral Pathol Oral Radiol 2012;114:1–8.
[12] Pessoa RS, Vaz LG, Marcantonio EJ, Vander Sloten J, Duyck J, Jaecques SV. Biomechanical evaluation of platform switching in different implant protocols: computed tomography-based three-dimensional finite element analysis. Int J Oral Maxillofac Implants 2010;25:911–9.
[13] Canay S, Akca K. Biomechanical aspects of bone-level diameter shifting at implant–abutment interface. Implant Dent 2009;18:239–48.
[14] Maeda Y, Miura J, Taki I, Sogo M. Biomechanical analysis on platform switching: is there any biomechanical rationale? Clin Oral Implants Res 2007;18:581–4.
[15] Tabata LF, Rocha EP, Barao VA, Assuncao WG. Platform switching: biomechanical evaluation using three-dimensional finite element analysis. Int J Oral Maxillofac Implants 2011;26:482–91.
[16] Kreis T. Handbook of holographic interferometry. Weinheim: Wiley-VCH; 2006.
[17] Schnars U, Jueptner WPO. Digital recording and numerical reconstruction of holograms. Meas Sci Technol 2002;13:85–101.
[18] Demoli N. Real-time monitoring of vibration fringe patterns by optical reconstruction of digital holograms: mode beating detection. Opt Express 2006;14:2117–22.
[19] Demoli N, Halaq H, Vukicevic D. White light reconstruction of image plane digital holograms. Opt Express 2010;18:12675–80.
[20] Chorres JE, Uono C, Gioso MA, Batista L, Muramatsu M, Campos TN. Qualitative analysis of stress distribution in tooth-implant and implant-supported prosthesis by means of holography interferometry method. RPG Rev Pós Grad 2005;12:412–6.
[21] Matsumoto T, Tamamura K, Sugimura T, Inada J. Holographic measurement on deformation of mandible with dental implants due to occlusion. Proc SPIE 1996;177:2922.
[22] Demoli N, Halaq H, Sariri K, Torzynski M, Vukicevic D. Undersampled digital holography. Opt Express 2009;17:15842–52.
[23] Kreis T. Holographic interferometry: principles and methods. Berlin: Akademie Verlag; 1996.
[24] Dittmer S, Dittmer MP, Kohorst P, Jendras M, Borchers L, Stiesch M. Effect of implant–abutment connection design on load bearing capacity and failure mode of implants. J Prosthodont 2011;20:510–6.
[25] Semper W, Heberer S, Mehrhof J, Schink T, Nelson K. Effects of repeated manual disassembly and reassembly on the positional stability of various implant–abutment complexes: an experimental study. Int J Oral Maxillofac Implants 2010;25:86–94.
[26] Al-Sukhun J, Helenius M, Lindqvist C, Kelleway J. Biomechanics of the mandible part I: measurement of mandibular functional deformation using custom-fabricated displacement transducers. J Oral Maxillofac Surg 2006;64:1015–22.
[27] Al-Sukhun J, Kelleway J. Biomechanics of the mandible: Part II. Development of a 3-dimensional finite element model to study mandibular functional deformation in subjects treated with dental implants. Int J Oral Maxillofac Implants 2007;22:455–66.
[28] Al-Sukhun J, Kelleway J, Helenius M. Development of a three-dimensional finite element model of a human mandible containing endosseous dental implants. I. Mathematical validation and experimental verification. J Biomed Mater Res A 2007;80:234–46.
[29] Moreno V, Vázquez-Vázquez C, Gallas M, Crespo J. Speckle shearing pattern interferometry to assess mechanical strain in the human mandible jaw bone under physiological stress. Proc SPIE 2011;8001:8001311–8.
[30] Baggi L, Cappelloni I, Di Girolamo M, Maceri F, Vairo G. The influence of implant diameter and length on stress distribution of osseointegrated implants related to crestal bone geometry: a three-dimensional finite element analysis. J Prosthet Dent 2008;100:422–31.
[31] Qian L, Todo M, Matsushita Y, Koyano K. Effects of implant diameter, insertion depth, and loading angle on stress/strain fields in implant/jawbone systems: finite element analysis. Int J Oral Maxillofac Implants 2009;24:877–86.
[32] Winter W, Klein D, Karl M. Micromotion of dental implants: basic mechanical considerations. J Med Eng 2013;2013:9.
[33] Ojeda J, Martinez-Reina J, Garcia-Aznar JM, Dominguez J, Doblare M. Numerical simulation of bone remodelling around dental implants. Proc Inst Mech Eng H 2011;225:897–906.
[34] Chou HY, Muftu S, Bozkaya D. Combined effects of implant insertion depth and alveolar bone quality on periimplant bone strain induced by a wide-diameter, short implant and a narrow-diameter, long implant. J Prosthet Dent 2010;104:293–300.